MNRAS **000**, 1–5 (2022) Preprint 21 September 2022 Compiled using MNRAS LATEX style file v3.0

Bayesian Analysis of Gas-free Galaxies in Simulations II: Progenitor Influences

Alexander Rawlings,[1]★ Others,[1]
[1] *Department of Physics, Gustaf Hällströmin katu 2, FI-00014, University of Helsinki, Finland*

Accepted XXX. Received YYY; in original form ZZZ

ABSTRACT
We present the Bayesian Analysis of Gas-free Galaxies in Simulations (BAGGinS) project, show that stochasticity is ubiquitous with collisionless merger sims.

Key words: keyword1 – keyword2 – keyword3

1 INTRODUCTION

Something cool

1.1 The KETJU Code

Basic overview and updates, refer to previous papers

1.2 Initial Conditions

We create four[1] unique progenitor galaxies, motivated by analogues observed in the real Universe. Each galaxy is modelled as a multi-component system: a stellar component embedded within a DM halo, and a single SMBH at rest at the centre of the galaxy. Two galaxies, A and D, have a stellar density profile given by the 'cuspy' Dehnen (1993) profile:

$$\rho_\star(r) = \frac{(3-\gamma)M_\star}{4\pi}\frac{a}{r^\gamma(r+a)^{(4-\gamma)}} \tag{1}$$

and two galaxies, C and E, by the 'cored' Terzić & Graham (2005) profile:

$$\rho_\star(r) = \rho'\left[1+\left(\frac{r_b}{r}\right)^\alpha\right]^{\gamma/\alpha} \times\left\{\left[\frac{r^\alpha+r_b^\alpha}{R_\mathrm{e}^\alpha}\right]^{-p/\alpha}\mathrm{e}^{-b\left[\left(r^\alpha+r_b^\alpha\right)/R_\mathrm{e}^\alpha\right]^{1/n\alpha}}\right\}, \tag{2}$$

where

$$\rho' = \rho_b 2^{(p-\gamma)/\alpha}\left(\frac{r_b}{r}\right)^p \mathrm{e}^{b\left(2^{1/\alpha}r_b/R_\mathrm{e}\right)^{1/n}}. \tag{3}$$

The stellar component, whilst having a spherically-symmetric density distribution, employs the anisotropic Osipkov-Merritt distribution function (DF), from which the phase space is Monte-Carlo sampled using a minimum of $\sim 10^6$ particles with a mass of $10^5\,\mathrm{M}_\odot$. The Osipkov-Merritt DF has a free parameter r_a, termed the anisotropy radius, which determines the degree of radial anisotropy. The DF is near-ergodic in the inner regions $r < r_a$, and becomes increasingly radially-biased at larger r. It has the form:

$$f(Q) = \frac{1}{\sqrt{8}\pi^2}\left[\int_0^Q \frac{\mathrm{d}\Psi}{\mathrm{d}\sqrt{Q-\Psi}}\frac{\mathrm{d}^2\nu_q}{\mathrm{d}\Psi^2} + \frac{1}{\sqrt{Q}}\left(\frac{\mathrm{d}\nu_Q}{\mathrm{d}\Psi}\right)_{\Psi=0}\right], \tag{4}$$

where

$$\nu_Q(r) \equiv \left(1+\frac{r^2}{r_a^2}\right)\nu(r)$$

and

$$Q \equiv \mathcal{E} - \frac{L^2}{2r_a^2}.$$

The parameter r_a is chosen so as to reproduce observed kinematic relations, most notably the $M_\bullet$–$\sigma_\star$ relation (see figure), whilst maintaining a positive DF.

Conversely, the DM halo of all galaxies is modelled as an ergodic Navarro-Frenk-White (NFW) profile (Navarro et al. 1997), with expected virial mass taken from the Behroozi et al. (2019) peak halo mass – stellar mass relation.

$$\rho_\mathrm{DM}(r) = \frac{\rho_0}{(r/a)(1+r/a)^2} \tag{5}$$

We do not incorporate a redshift-dependent halo mass, instead opting to model our haloes as if they were taken at $z = 0$. The NFW concentration parameter $c \equiv r_\mathrm{vir}/a$, where a is the scale radius, is taken from the Dutton & Macciò (2014) relation. To prevent the radially-divergent mass distribution associated with the NFW profile, we multiply the density profile Equation 5 with a sigmoid function, and demand that the ratio of the actual DM density to the theoretical NFW density satisfies

$$\frac{\rho_\mathrm{true}(r)}{\rho_\mathrm{NFW}(r)} < 10^{-5}$$

by 7 R_vir, with significant departure from the NFW profile already

★ E-mail: alexander.rawlings@helsinki.fi
[1] A fifth galaxy, model B, was created with much higher mass than the four presented here. As the merger system did not result in a bound SMBH binary within some 10 Gyr, we exclude discussion of this galaxy.

Table 1. Properties of progenitor galaxies

Name	Stellar Profile	r_a/kpc	$M_\star/(10^{11}\,M_\odot)$	$N_\star$	$M_{\rm DM}/(10^{13}\,M_\odot)$	$c_{\rm DM}$	$N_{\rm DM}$	$M_\bullet/(10^9\,M_\odot)$	$R_{\rm vir}$/kpc	$R_{\rm e}$/kpc
A	Dehnen	0.4	2.51	2.5×10^6	9.65	7.55	3.22×10^6	3.04	554	4.40
C	Terzić	1.5	2.57	2.6×10^6	5.13	7.51	3.38×10^6	3.14	562	4.05
D	Dehnen	0.3	1.58	1.58×10^6	2.00	8.23	1.29×10^6	1.64	412	3.16
E	Terzić	0.5	1.46	1.46×10^6	3.29	8.36	1.10×10^6	1.46	392	2.79

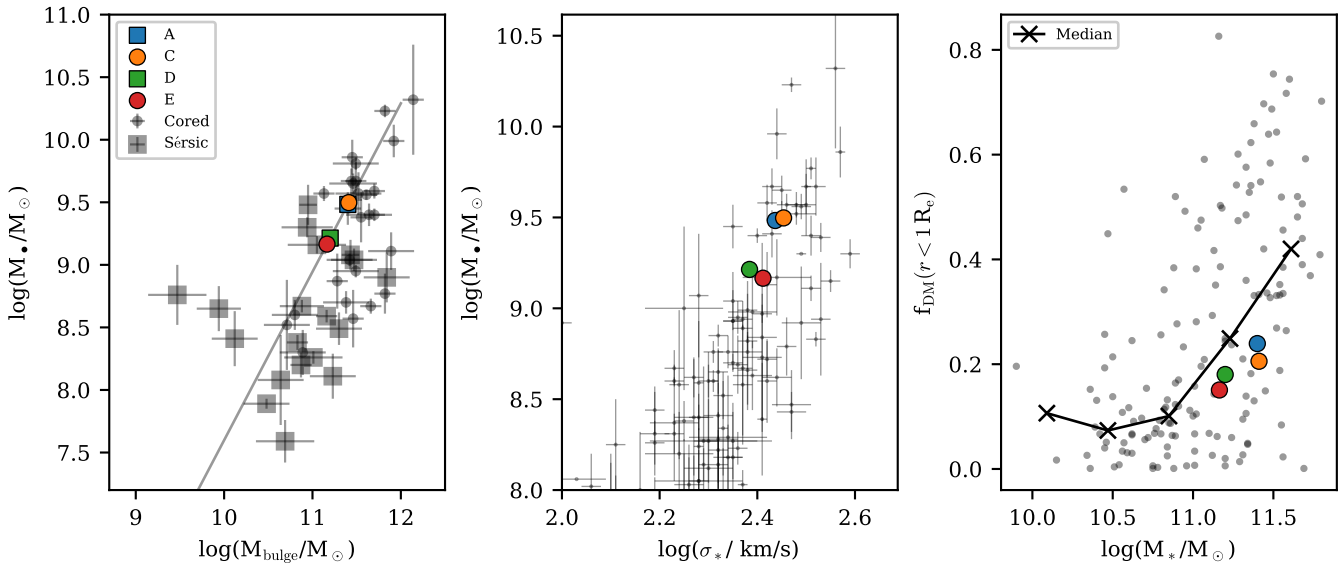

Figure 1. Comparison of progenitor galaxies to key observables. *Left:* The simulated galaxies have a SMBH mass determined from the Sahu et al. (2019) relation. Cored galaxies are shown as circles, and cuspy galaxies as squares. Note the progenitor galaxies A and C overlap. *Centre*: The stellar velocity dispersion within 1 $R_{\rm e}$ is computed for the progenitor galaxies, and compared to observational data collated in van den Bosch (2016). *Right:* The dark matter fraction within 1 $R_{\rm e}$ is computed for the progenitor galaxies, and compared to Schwarzschild-modelling results from Jin et al. (2020).

by 3 $R_{\rm vir}$. With this modified NFW profile, the phase space is Monte Carlo sampled using the approach of Equation 4 and a minimum of $\sim 10^6$ particles with a mass of $3.0\times10^7\,{\rm M}_\odot$, assuming $L = 0$ and $r_a \rightarrow \infty$. The virial radius of the system is then re-determined numerically, to ensure it is in close agreement with the expected value from Behroozi et al. (2019).

The final component of the model galaxies, the SMBH, is represented as a point mass at rest at the origin. The SMBH mass is taken from the $M_{\rm bulge}$–$M_\bullet$ relation of Sahu et al. (2019), and by definition lies on this relation, shown in the left panel of Figure 1. The SMBH is also given an initial spin χ from the Lousto et al. (2010) distribution, so that we may also investigate GW-induced recoil kicks in our merger remnants.

We compare the progenitor systems to key constraining observables in Figure 1. In the centre panel, we overlay our progenitor galaxies on data used to fit the black hole mass - central stellar velocity dispersion relation of van den Bosch (2016). The progenitor galaxies lie within the spread of the data, and have velocity dispersions indistinguishable from observational data. Similarly, we find that the fraction of dark matter within 1 $R_{\rm e}$ is comparable to the dark matter fraction determined with Schwarzschild modelling of central and satellite galaxies in the MaNGA survey (Jin et al. 2020), shown in the right panel of Figure 1. Our progenitor galaxies are consistently slightly below the median relation (the median $f_{\rm DM}$ value is shown as crosses in stellar mass bins), but still well within the scatter of Jin et al. (2020). We conclude that our progenitor galaxy models, whilst neglecting the inclusion of gas, plausibly represent observable massive galaxies, particularly at the mass range of $M_\star/M_\odot > 10^{11}$ that we are interested in.

After creating and assessing the multicomponent ICs, the galaxies are evolved in isolation using Gadget-3 for at least 8 Gyr , to ensure the systems are fully-relaxed and any potential effects arising from radial instabilities are mitigated. We then extract the evolved systems, and align each system with its reduced inertia tensor. We use these as the progenitor galaxies for all subsequent merger configurations.

1.3 Simulations

We simulate all six different progenitor combinations, namely AC, AD, AE, CD, CE, DE. This allows us to sample a vast range of progenitor configurations: each of equal and unequal mass, for each combination of cuspy and cored profiles. Herein, we refer to a particular progenitor combination as a *progenitor class*.

In keeping with our theme of realistic initial conditions, we set all galaxy merger orbits to an initial separation of $r_0 = 3\,R_{\rm vir,1}$, where $R_{\rm vir,1}$ is the virial radius of the larger of the two progenitors. The progenitor galaxies are then set on a quasi-Keplerian orbit, assuming each galaxy is a point-mass containing half its total mass. The eccentricity of the initial orbit is chosen as a function of the

initial pericentre distance $r_{\rm peri}$, motivated from cosmological simulations, using the data presented in Khochfar & Burkert (2006). By fitting a functional form to the median eccentricity value in logarithmically-spaced bins, we arrive at the relation

$$e(r_{\rm peri}/R_{\rm vir,1}) = \left[1 + \left(\frac{r_{\rm peri}/R_{\rm vir,1}}{0.320}\right)^{1.629}\right]^{-0.176} \quad (6)$$

from which we set the initial eccentricity of all our merger orbits. For each progenitor class, we sample six different pericentre distances, and thus six different eccentricities, in the range $10^{-3} \leq r_{\rm peri}/R_{\rm vir,1} \leq 1.0$. Consequently, we investigate 36 'families' of merger configurations.

The integration of the system is conducted in two phases: a *parent phase* and a *child phase*. The former is done to capture the large-scale dynamics when the SMBHs are at large separation, and the latter when the SMBH interactions become of primary interest.

The progenitors are evolved through the *parent phase* from $t(r_0) = 0$ with Gadget-3 until the SMBHs form a bound binary at $t_{\rm stop}$, with a stellar softening of $\epsilon_\star = 10\,$pc and Gadget-3 integration tolerances `ErrTolIntAccuracy`=0.02 and `ErrTolForceAcc`=0.005. We then initialise the *child phase* by restarting from a snapshot sometime before $t_{\rm stop}$. We apply a small perturbation to each SMBH position and velocity vector to mimic the effect of Brownian motion due to discrete sampling of the DF, thus negating the need to run many simulations from $r_0 = 3\,R_{\rm vir,1}$. The perturbations are drawn from a Gaussian distribution modelling the typical offset of the SMBH phase space coordinates from the phase space coordinates of the stellar centre of mass, determined using the shrinking sphere method. The Gaussian distributions are characterised by $\mathcal{N}_{\rm pos}(\mu = 0\,{\rm pc}, \sigma^2 = 100\,{\rm pc}^2)$, and $\mathcal{N}_{\rm vel}(\mu = 0\,{\rm km\,s^{-1}}, \sigma^2 = 100\,{\rm km^2\,s^{-2}})$ for each progenitor should we show a figure of this? . From each *parent* , we create ten uniquely-perturbed *child* runs, allowing us to explore the distribution of parameters describing both the orbital and remnant properties of each *parent* merger. Additionally, we lower the stellar softening to $\epsilon_\star = 3.5\,$pc and tighten the integration tolerance `ErrTolIntAccuracy` to 0.002 to optimise the run for Ketju . We check for energy conservation between the *parent* and *child* runs, and confirm that the total energy is conserved at the sub-percent level. In total, we perform 360 ultra-high resolution unique *child* simulations using Ketju , and use this sample for our analysis.

Within a relatively short time frame from beginning the *child* run, the SMBH binary hardens predominantly through three-body stellar interactions. We evolve the binary to the time $t_{a_h} = t(a_h)$, and continue to when $t_{\rm safe} = t(a = 15\,{\rm pc})$. We then analytically predict the orbital evolution of the binary by determining the hardening constant assume this was explained in the intro H and eccentricity constant K by fitting the derivative of $\mathrm{d}(1/a)/\mathrm{d}t$ with a linear function between t_{a_h} and $t_{\rm safe}$. Using $a_0 = a_h$ and three different values of e_0, taken to be the 5%, 50%, and 95% quantiles of the eccentricity distribution with the same time interval $t_{a_h} - t_{\rm safe}$, we predict the expected merger timescale of the system. We continue to run the *child* runs until one of three conditions are met:

(i) The SMBHs merge, or
(ii) The Hubble time, 13.8 Gyr, is exceeded, or
(iii) The eccentricity stabilises to below the analytically-determined eccentricity estimated from the 5%-quantile eccentricity value, and said analytical-estimate indicates that the merger will occur significantly after the Hubble time.

[t]

Table 2. Properties of merger orbits

Name	$r_{\rm peri}/R_{\rm vir,1}$	e_0
XY-030-0001	1.0×10^{-3}	0.999
XY-030-0005	5.0×10^{-3}	0.998
XY-030-0010	1.0×10^{-2}	0.994
XY-030-0050	5.0×10^{-2}	0.992
XY-030-0100	1.0×10^{-1}	0.976
XY-030-1000	1.0×10^{0}	0.703

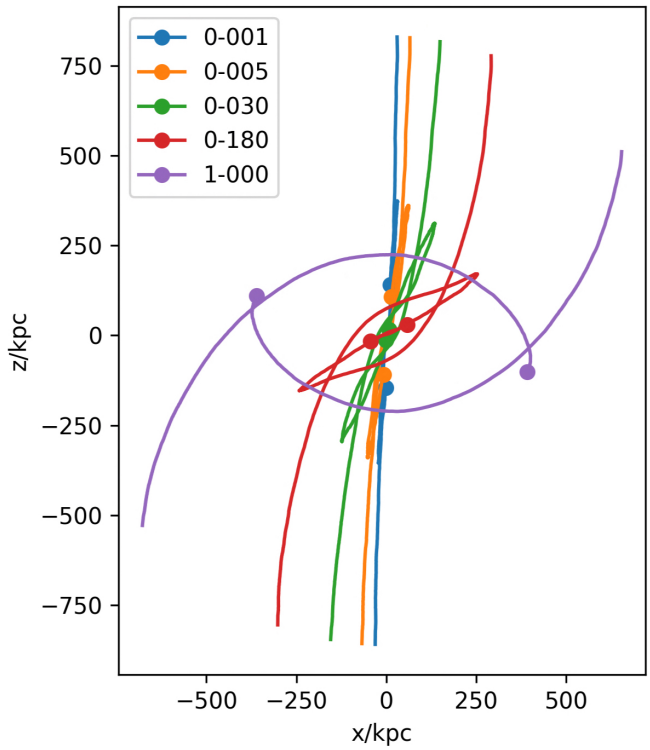

Figure 2. Plots of the initial orbit? Update this figure if so

If it is not clear if the third condition is satisfied, we continue to run the merger until the second condition is met.

2 STATISTICAL ANALYSIS

Include HM method here

3 RESULTS

Have some nice plots, groundbreaking results

4 DISCUSSION

Discuss said groundbreaking results

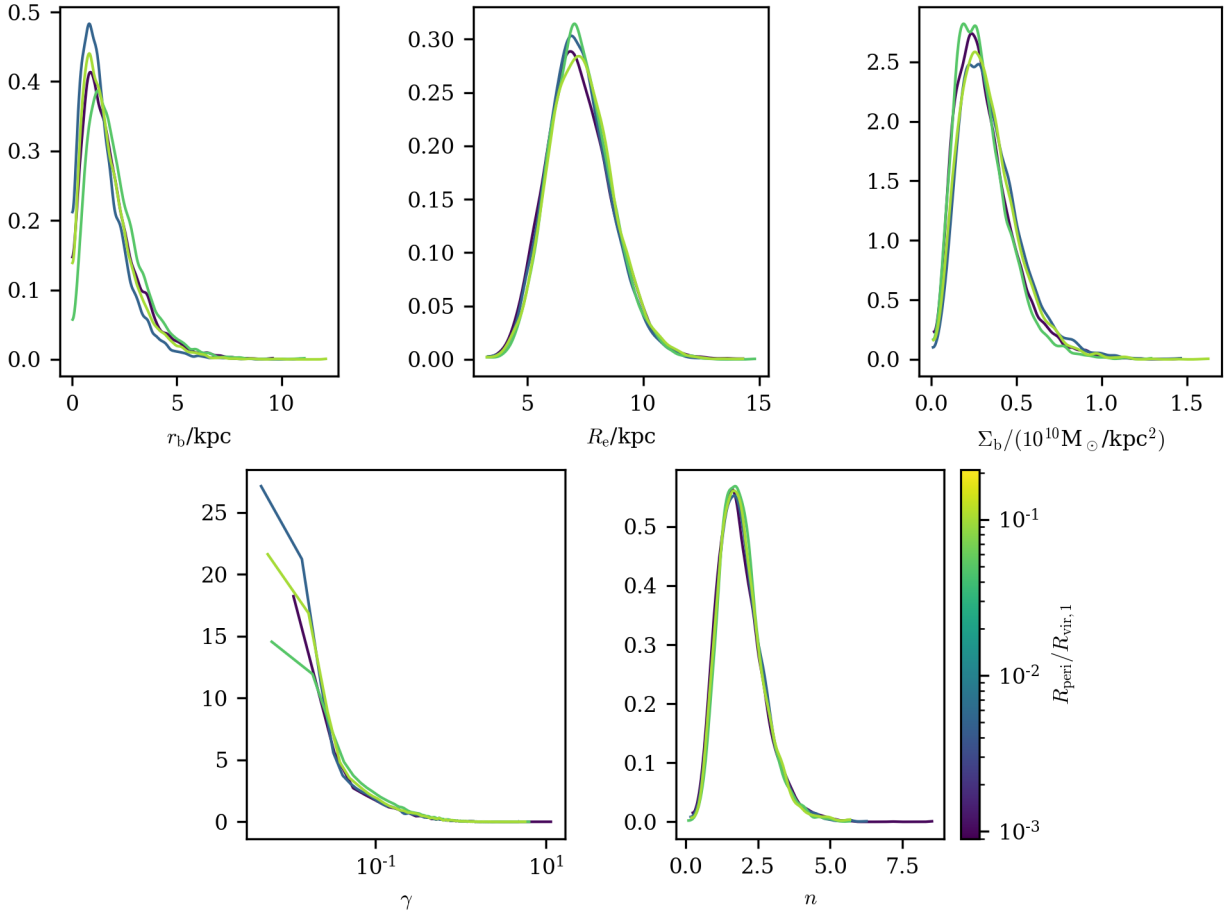

Figure 3. Comparing the latent parameters for different members of the same progenitor class. Here shown is those families part of the (approximately equal-mass) AC merger class. There is no significant difference in latent parameter values with increasing rperi. TODO do this same plot for each merger class.

5 CONCLUSIONS

Leave the reader with a good feeling

Software: Ketju (Rantala et al. 2017), Gadget-3 (Springel 2005), Stan (Carpenter et al. 2017), NumPy (Harris et al. 2020), SciPy (Virtanen et al. 2020), Matplotlib (Hunter 2007), pygad (Röttgers et al. 2020), Arviz (Kumar et al. 2019).

ACKNOWLEDGEMENTS

P.H.J. acknowledge the support by the European Research Council via ERC Consolidator Grant KETJU (no. 818930).

The numerical simulations used computational resources provided by the CSC – IT Center for Science, Finland.

DATA AVAILABILITY

The inclusion of a Data Availability Statement is a requirement for articles published in MNRAS. Data Availability Statements provide a standardised format for readers to understand the availability of data underlying the research results described in the article. The statement may refer to original data generated in the course of the study or to third-party data analysed in the article. The statement should describe and provide means of access, where possible, by linking to the data or providing the required accession numbers for the relevant databases or DOIs.

REFERENCES

Behroozi P., Wechsler R. H., Hearin A. P., Conroy C., 2019, MNRAS, 488, 3143
Carpenter B., et al., 2017, Journal of Statistical Software, 76, 1
Dehnen W., 1993, MNRAS, 265, 250
Dutton A. A., Macciò A. V., 2014, MNRAS, 441, 3359
Harris C. R., et al., 2020, Nature, 585, 357
Hunter J. D., 2007, Computing in Science & Engineering, 9, 90
Jin Y., Zhu L., Long R. J., Mao S., Wang L., van de Ven G., 2020, MNRAS, 491, 1690
Khochfar S., Burkert A., 2006, A&A, 445, 403
Kumar R., Carroll C., Hartikainen A., Martin O., 2019, Journal of Open Source Software, 4, 1143
Lousto C. O., Nakano H., Zlochower Y., Campanelli M., 2010, Phys. Rev. D, 81, 084023
Navarro J. F., Frenk C. S., White S. D. M., 1997, ApJ, 490, 493
Rantala A., Pihajoki P., Johansson P. H., Naab T., Lahén N., Sawala T., 2017, ApJ, 840, 53
Röttgers B., Naab T., Cernetic M., Davé R., Kauffmann G., Borthakur S., Foidl H., 2020, MNRAS, 496, 152
Sahu N., Graham A. W., Davis B. L., 2019, ApJ, 876, 155
Springel V., 2005, MNRAS, 364, 1105
Terzić B., Graham A. W., 2005, MNRAS, 362, 197

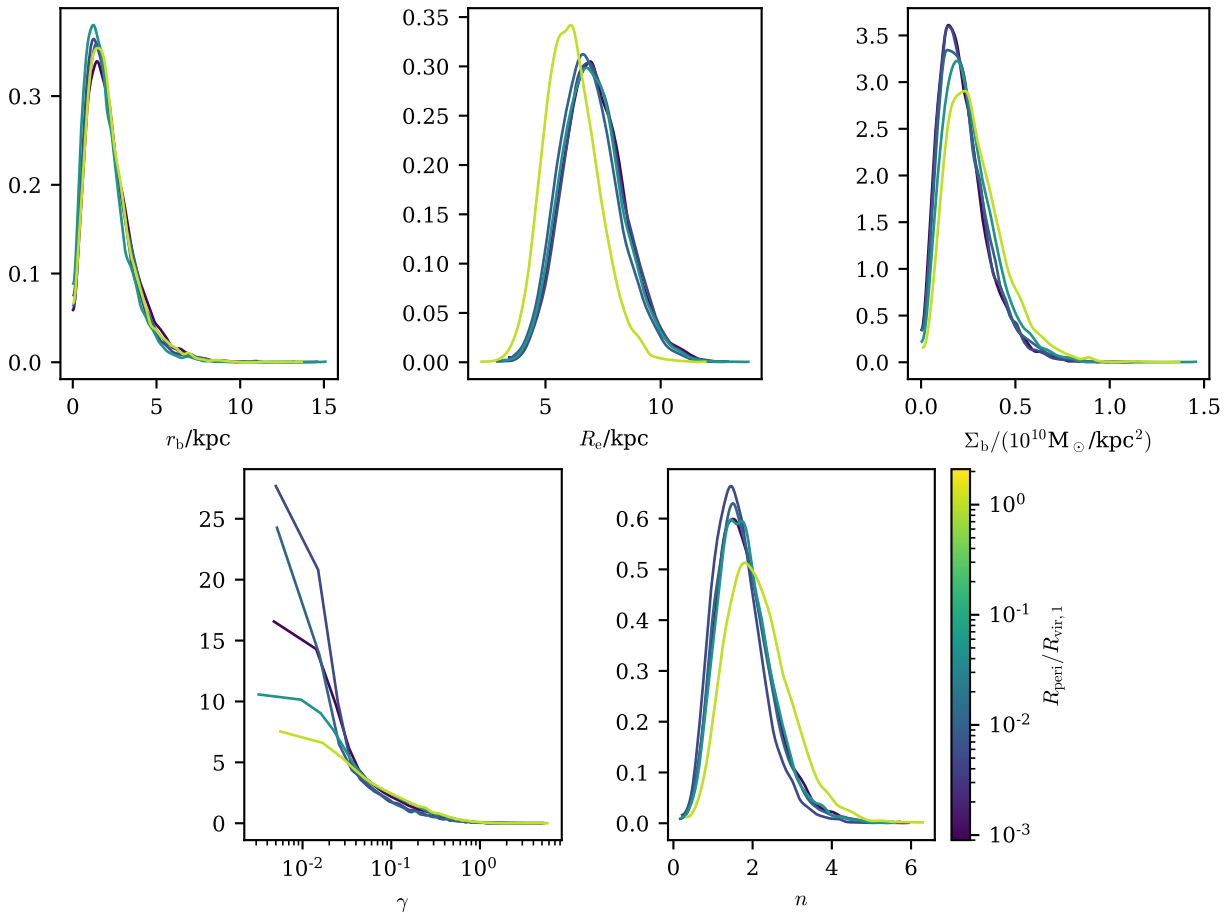

Figure 4. Same as Figure 3, but for the (unequal mass) AD merger class. For merger families with $R_{peri}/R_{vir,1} \leq 0.1$, the latent parameter distributions are indistinguishable. COnversely, for the A-D-3.0-1.0 family, the effective radius has its mode at lower values than the other merger class members, and its Sérsic index peaks at slightly higher values of n.

Virtanen P., et al., 2020, Nature Methods, 17, 261
van den Bosch R. C. E., 2016, ApJ, 831, 134

APPENDIX A: SOME EXTRA MATERIAL

If you want to present additional material which would interrupt the flow of the main paper, it can be placed in an Appendix which appears after the list of references.

This paper has been typeset from a TEX/LATEX file prepared by the author.